Optimal partially superimposed pilot pattern for OTFS communication

Rabah Ouchikh, Abdeldjalil Aissa El Bey, Thierry Chonavel, Nacerredine Lassami

Optimal partially superimposed pilot pattern for OTFS communication

Rabah Ouchikh
Lab Télécommunications
Ecole Militaire Polytechnique
Bordj El-Bahri, Algeria
ouchikh16rabah@gmail.com

Abdeldjalil Aïssa-El-Bey
IMT Atlantique, Lab-STICC,
UMR CNRS 6285, F-29238,
Brest, France
abdeldjalil.aissaelbey@imt-atlantique.fr

Thierry Chonavel
IMT Atlantique, Lab-STICC,
UMR CNRS 6285, F-29238,
Brest, France
thierry.chonavel@imt-atlantique.fr

Nacerredine Lassami
Lab Traitement du signal
Ecole Militaire Polytechnique
Bordj El-Bahri, Algeria
lassami.nacerredine@gmail.com

***Abstract*—This paper tackles the intricate challenge of channel estimation (CE) and symbol detection in high-mobility scenarios for orthogonal time frequency space (OTFS) systems. We introduce a novel partially superimposed pilots (PSP) pattern, strategically balancing computational complexity and CE accuracy by partially superimposing pilots and data symbols in the delay-Doppler (DD) domain. Additionally, we propose a CE and symbol detection (CESD) algorithm, employing an iterative approach that combines low complexity minimum mean squared error (LMMSE) for CE and simplicity-based detection for data symbols. Key contributions encompass optimal pilot pattern determination, a comprehensive iterative algorithm, and a thorough performance evaluation. Comparative analyses with state-of-the-art methods underscore the superior trade-off achieved by CESD in terms of normalized mean square error for CE, bit error rate, spectral efficiency, and computational complexity.**

***Index Terms*—OTFS, Channel estimation, Symbol detection, LMMSE, Simplicity, Pilot pattern.**

I. Introduction

Future mobile communication systems encounter a significant challenge in ensuring reliable communication within high-mobility scenarios. However, the widely used orthogonal frequency division multiplexing (OFDM) modulation faces performance degradation under such conditions [1]. Orthogonal time frequency space (OTFS) modulation, is designed to address this challenge by effectively managing time-varying channels [2]. OTFS convert a doubly-selective wireless channel into an almost flat one within the delay-Doppler (DD) domain. To ensure resilient data transmission in an OTFS system, the development of efficient channel estimation (CE) and data detection algorithms becomes imperative.

Various CE approaches for OTFS in the DD domain fall into three main categories. The first category involves conventional pilot-aided (CPA) schemes using the initial frame handles CE, while subsequent frames are dedicated to data detection [3]. The second category, known as embedded pilots (EP), integrates CE and data detection within the same frame [1], [4]–[7]. This is achieved by interleaving pilots and data symbols on the same DD grid, incorporating guard intervals (GI) to prevent interference. The third category encompasses schemes that superimposed pilots and data symbols in the DD domain [8]–[10]. This category necessitates advanced iterative algorithms for effective CE and precise data detection.

This paper introduces a novel pilot insertion strategy, named partially superimposed pilots (PSP), in the OTFS framework. As shown in Fig. 1c, PSP superimposes pilots and data symbols in a portion of the DD grid, striking a balance between computational complexity and CE accuracy. This approach aims to find an optimal pilot number, offering a compromise between the single superimposed pilots (SSP) and fully superimposed pilots (FSP) schemes, shown in Fig. 1a and Fig. 1b, respectively. SSP minimizes interference by superimposing a single pilot with a data symbol, employing a threshold method for CE. However, it faces challenges related to a high peak-to-average power ratio (PAPR). On the other hand, FSP resolves the PAPR issue by superimposing all pilots across the entire DD grid but introduces additional computational complexity, requiring an iterative algorithm for efficient CE and data detection. In conjunction with the proposed pilot pattern, we present a novel CE and symbol detection (CESD) algorithm for OTFS systems. CESD iterates between LMMSE-based CE and Simplicity-based symbol detection [11].

The main contributions of this paper are:

- The determination of the optimal number of pilots that allows for efficient detection while reducing the complexity of channel estimation computation.
- The proposal of an iterative algorithm for CE and symbol detection, utilizing the proposed pilot pattern along with LMMSE-based CE and simplicity-based detection.
- The performance evaluation showcases the favourable balance achieved by the algorithm between bit error rate (BER), spectral efficiency (SE), and computational complexity when compared to state-of-the-art methods.

Notation: $\odot$ and $\otimes$ represent the Hadamard product and the Kronecker product. The column vectorization of an $M \times N$ matrix and the invectorization of an MN column vector are denoted as $\mathrm{vec}(.)$ and $\mathrm{vec}^{-1}(.)$. $\mathcal{CN}(m, \sigma^2)$ denotes the circular complex Gaussian distribution with mean m and variance σ^2. $\mathrm{diag}\{d_1, d_2, ..., d_N\}$ represents an $N \times N$ diagonal matrix with diagonal entries $d_1, d_2, ..., d_N$. Finally, $\boldsymbol{I}_M$, $\boldsymbol{F}_n$, and $\boldsymbol{F}_n^H$ stand for the $M \times M$ identity matrix, the n-point discrete Fourier transform (DFT) matrix, and the conjugate transpose of the n-point DFT matrix.

II. OTFS WITH PSP SCHEME

We are examining a single-input single-output OTFS system. The DD grid is segmented into N symbols and M subcarriers. Here, Δf, $B = M\Delta f$, and $T_f = NT$ represent the subcarrier spacing, bandwidth, and frame duration, respectively. Additionally, it is given that $T\Delta f = 1$.

Using the PSP scheme, the Tx DD signal $\boldsymbol{X}$ is given as: $\boldsymbol{X}[k,l] = \boldsymbol{X}_p[k,l] + \boldsymbol{X}_d[k,l]$ for $k \in [k_p - N_p, k_p + N_p]$, $l \in [l_p, l_p + M_p - 1]$ and $\boldsymbol{X}[k,l] = \boldsymbol{X}_d[k,l]$ otherwise, where $\boldsymbol{X}_p \in \mathbb{C}^{M\times N}$ is constructed with pilots within the sub-grid $[l_p, l_p + M_p - 1] \times [k_p - N_p, k_p + N_p]$ and zeros elsewhere. On the other hand, $\boldsymbol{X}_d \in \mathbb{C}^{M\times N}$ holds data symbols in all DD positions. The coordinates (k_p, l_p) indicate the central pilot location. To achieve good CE, the size of pilot signals should cover the maximum delay and Doppler spread, meaning $M_p \geq l_\tau$, and $2N_p + 1 \geq k_\nu$. Therefore, the values of M_p and N_p are meticulously chosen to find the right balance between CE accuracy and computational complexity.

The DD domain signal $\boldsymbol{X}$ is first converted to the time-frequency domain $\boldsymbol{X}_{TF}$ by the ISFFT and the window function. The OTFS Tx time domain signal is then formed by applying the Heisenberg transform to $\boldsymbol{X}_{TF}$, yielding

$$\boldsymbol{s} = (\boldsymbol{F}_N^H \otimes \boldsymbol{I}_M)\boldsymbol{x}, \tag{1}$$

where $\boldsymbol{x} = \text{vec}(\boldsymbol{X})$. A cyclic prefix (CP) is appended to $s(t)$ before it is transmitted to prevent inter-symbol interference.

The signal $s(t)$ passes through the sparse P-path DD time-varying channel with the given impulse response:

$$h(\tau,\nu) = \sum_{i=1}^{P} h_i \delta\left(\tau - l_i/M\Delta f\right)\delta\left(\nu - k_i/NT\right), \tag{2}$$

where h_i, l_i, and k_i are, respectively, the complex gain, the delay and Doppler taps for the i-th path. The delays and Doppler shifts are integer multiples of the sampling period.

After removing the CP, the Rx signal $\boldsymbol{r}$ is given. The Wigner transform and the SFFT are applied to $\boldsymbol{r}$, resulting in

$$\boldsymbol{y} = (\boldsymbol{F}_N \otimes \boldsymbol{I}_M)\boldsymbol{r}, \tag{3}$$

where $\boldsymbol{r} = \boldsymbol{H}\boldsymbol{s} + \boldsymbol{v}$. $\boldsymbol{v} \sim \mathcal{CN}(0,\sigma^2)$, and $\boldsymbol{H} = \sum_{i=1}^{P} h_i \boldsymbol{\Pi}^{l_i}\boldsymbol{\Delta}^{(k_i)}$. Here, $\boldsymbol{\Pi}$ is the shift permutation matrix, $\boldsymbol{\Delta} = \text{diag}\{\exp(j2\pi(0)/MN), ..., \exp(j2\pi(MN-1)/MN)\}$.

Upon substituting the expression of $\boldsymbol{r}$ into (3), $\boldsymbol{y}$ can be related to, $\boldsymbol{x}_d = \text{vec}(\boldsymbol{X}_d)$, and $\boldsymbol{x}_p = \text{vec}(\boldsymbol{X}_p)$ by

$$\boldsymbol{y} = \boldsymbol{H}_{\text{eff}}\boldsymbol{x} + \boldsymbol{n} = \boldsymbol{H}_{\text{eff}}\boldsymbol{x}_d + \boldsymbol{H}_{\text{eff}}\boldsymbol{x}_p + \boldsymbol{n}, \tag{4}$$

where $\boldsymbol{H}_{\text{eff}} = (\boldsymbol{F}_N \otimes \boldsymbol{I}_M)\boldsymbol{H}(\boldsymbol{F}_N^H \otimes \boldsymbol{I}_M)$, and $\boldsymbol{n} = (\boldsymbol{F}_N \otimes \boldsymbol{I}_M)\boldsymbol{v} \sim \mathcal{CN}(0,\sigma^2)$.

The goal is to estimate the channel parameters $(l_i, k_i, h_i)_{i=1:P}$. Contrastingly, symbol detection involves determining $\boldsymbol{x}_d$ from (4). Since $\{l_i, k_i\}$ remain unchanged for a period T_s, for a doubly-underspread (DU) channel, the estimation of these parameters is done once every $T_s = N_T T$ seconds, where N_T is the number of frames in the period T_s.

III. PROPOSED ALGORITHM

Figure 1d shows the Rx pattern for the PSP scheme. Elements represented by a blue square inside a red circle represent the signal containing pilots and data symbols which are used for CE. Elements represented by a red circle inside a blue square represent data symbols affected by pilots. Once the channel is estimated, an interference cancellation (IC) scheme is executed to remove the pilot contribution from the data. The blue squares designate data symbols unaffected by pilots.

A. Non iterative algorithm (NIA)

Here, we introduce the proposed non-iterative algorithm (NIA) for CE and symbol detection.

To estimate the channel, we utilize $K = (2N_p + 1)M_p$ pilots. It is noteworthy that the number of pilots K will be determined subsequently to ensure a good trade-off between computational complexity and the efficiency of CE. The received vector $\boldsymbol{y}_p \in \mathbb{C}^{K\times 1}$ for $l_p \leq l \leq l_p + M_p - 1$ and $k_p - N_p \leq k \leq k_p + N_p$ can be expressed as

$$\boldsymbol{y}_p = \boldsymbol{A}_p\boldsymbol{h} + \boldsymbol{A}_d\boldsymbol{h} + \tilde{\boldsymbol{n}}, \tag{5}$$

where $\boldsymbol{A}_p$, $\boldsymbol{A}_d \in \mathbb{C}^{K\times P}$ denote the pilot matrix and the matrix containing $K \times P$ from the MN data symbols. $\boldsymbol{h} = [h_1, h_2, ..., h_P]^T \in \mathbb{C}^{P\times 1} \sim \mathcal{CN}(\boldsymbol{0}, \text{diag}\{\sigma^2_{h_1}, \sigma^2_{h_2}, ..., \sigma^2_{h_P}\})$.

By treating data as interference, the received signal in (5) can be reformulated as follows:

$$\boldsymbol{y}_p = \boldsymbol{A}_p\boldsymbol{h} + \tilde{\boldsymbol{n}}_d, \tag{6}$$

where $\tilde{\boldsymbol{n}}_d = \boldsymbol{A}_d\boldsymbol{h} + \tilde{\boldsymbol{n}} \sim \mathcal{CN}(\boldsymbol{0}, ((\sum_{i=1}^{P}\sigma^2_{h_i})\sigma_d^2 + \sigma^2)\boldsymbol{I}_K)$.

Using the observation model (6), we obtain the estimate $\hat{\boldsymbol{h}}_{\text{NIA}}$ for $\boldsymbol{h}$ through an LMMSE estimator, given by:

$$\hat{\boldsymbol{h}}_{\text{NIA}} = (\boldsymbol{A}_p^H\boldsymbol{C}^{-1}_{\tilde{\boldsymbol{n}}_d}\boldsymbol{A}_p + \boldsymbol{C}^{-1}_{\boldsymbol{h}})^{-1}\boldsymbol{A}_p^H\boldsymbol{C}^{-1}_{\tilde{\boldsymbol{n}}_d}\boldsymbol{y}_p. \tag{7}$$

Note that this estimation capitalizes on the sparsity in the DD domain by inverting a $P \times P$ matrix, with $P \ll MN$.

Once the channel is estimated, an IC scheme is employed to eliminate the contribution of pilots on data symbols before the data detection step. Thus, the signal used for symbol detection is obtained as follows:

$$\boldsymbol{y}_d = \boldsymbol{y} - \hat{\boldsymbol{H}}_{\text{eff}}\boldsymbol{x}_p = \boldsymbol{H}_{\text{eff}}\boldsymbol{x}_d + \tilde{\boldsymbol{n}}_e, \tag{8}$$

where $\tilde{\boldsymbol{n}}_e = (\boldsymbol{H}_{\text{eff}} - \hat{\boldsymbol{H}}_{\text{eff}})\boldsymbol{x}_p + \boldsymbol{n}$.

Now, the signal $\boldsymbol{y}_d$ in (8) will be utilized to determine the data symbols vector $\boldsymbol{x}_d$ using a simplicity-based detector.

The entries of $\boldsymbol{x}_d$ belong to an M-QAM modulation alphabet denoted by $\mathcal{A} = \{a_1, a_2, ..., a_M\}$, where $a_i = \alpha_i + j\beta_i$, $i \in \{1, ..., M\}$ with $(\alpha_i, \beta_i) \in \mathcal{F} \times \mathcal{F}$. Then, equation (8) is equivalent to the following real-valued system model:

$$\underline{\boldsymbol{y}_d} = \underline{\boldsymbol{H}_{\text{eff}}\boldsymbol{x}_d} + \underline{\tilde{\boldsymbol{n}}_e}, \quad \underline{\boldsymbol{x}_d} \in \mathcal{F}^{2MN}, \tag{9}$$

where $\underline{\boldsymbol{y}_d} = [\Re[\boldsymbol{y}_d], \Im[\boldsymbol{y}_d]]^T$, $\underline{\tilde{\boldsymbol{n}}_e} = [\Re[\tilde{\boldsymbol{n}}_e], \Im[\tilde{\boldsymbol{n}}_e]]^T$, and

$$\underline{\boldsymbol{H}_{\text{eff}}} = \begin{pmatrix} \Re[\boldsymbol{H}_{\text{eff}}] & -\Im[\boldsymbol{H}_{\text{eff}}] \\ \Im[\boldsymbol{H}_{\text{eff}}] & \Re[\boldsymbol{H}_{\text{eff}}] \end{pmatrix}. \tag{10}$$

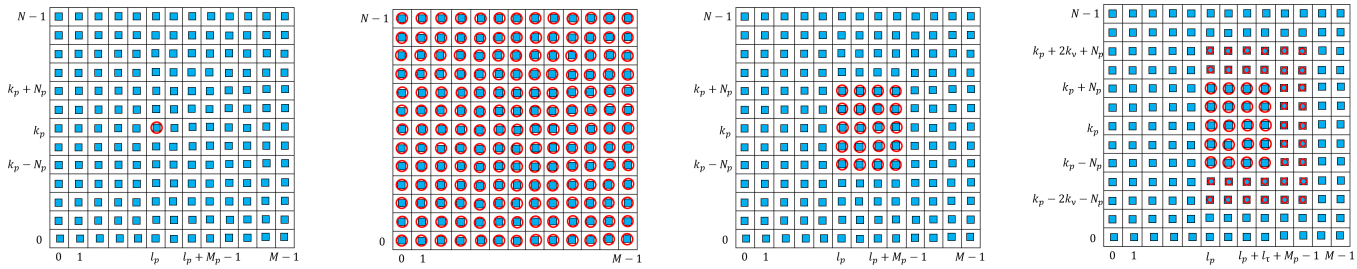

(a) SSP scheme (Tx). (b) FSP scheme (Tx). (c) Proposed PSP scheme (Tx). (d) Proposed PSP scheme (Rx).

Fig. 1: Tx and Rx patterns in the DD domain (○: pilot symbol, ■: data symbol).

Our problem is the recovery of $\underline{\boldsymbol{x}_d}$ from $\underline{\boldsymbol{y}_d}$ given $\underline{\boldsymbol{H}_{\text{eff}}}$ and $\mathcal{F}$. The maximum likelihood (ML) problem reads

$$\underline{\hat{\boldsymbol{x}}_d} = \arg\min_{\underline{\boldsymbol{x}_d}} ||\underline{\boldsymbol{y}_d} - \underline{\boldsymbol{H}_{\text{eff}}}\underline{\boldsymbol{x}_d}||_2 \text{ subject to } \underline{\boldsymbol{x}_d} \in \mathcal{F}^{2MN}. \tag{11}$$

Solving this problem is NP-hard. To address this challenge, we propose a detector based on the signal simplicity as in [11]. The signal is defined to be simple if the majority of its elements are equal to the extremes of the finite alphabet [12].

Therefore, the issue of the finite alphabet constraint as presented in (11) can be alleviated by relaxing it to a convex box constraint, depending only on the constellation extremes $\{\alpha_1, \alpha_m\}$ (e.g., $\{-1, +1\}$ for BPSK or $\{-3, +3\}$ for 16-QAM modulation). The relaxed optimization problem for the determination of $\underline{\boldsymbol{x}_d}$ is formulated as follows:

$$\hat{\boldsymbol{g}} = \arg\min_{\boldsymbol{g}} ||\underline{\boldsymbol{y}_d} - \underline{\boldsymbol{H}_{\text{eff}}}\boldsymbol{B}_\alpha \boldsymbol{g}||_2 \text{ subject to } \boldsymbol{B}_1\boldsymbol{g} = \boldsymbol{1}_{2MN}, \boldsymbol{g} \geq 0. \tag{12}$$

where $\boldsymbol{g} \in \mathbb{R}^{4MN}$ is the sparse transform of $\underline{\boldsymbol{x}_d}$: $\underline{\boldsymbol{x}_d} = \boldsymbol{B}_\alpha \boldsymbol{g}$. $\boldsymbol{B}_\alpha = \boldsymbol{I}_{2MN} \otimes [\alpha_1, \alpha_m]$, $\boldsymbol{B}_1 = \boldsymbol{I}_{2MN} \otimes [1, 1]$.

In addition to the convexity of this formulation, the computation cost of the resulting detector does not depend on the constellation size $|\mathcal{A}|$. Please note that the efficiency of this approach is determined by the number of points enclosed within the square box delineated by the constellation boundary.

We solve this problem using the point interior method. Once $\boldsymbol{g}$ is obtained, the real-valued vector $\underline{\boldsymbol{x}_d}$ can be obtained as $\underline{\boldsymbol{x}_d} = \boldsymbol{B}_\alpha \boldsymbol{g}$. Then, $\boldsymbol{x}_d$ can be easily obtained from $\underline{\boldsymbol{x}_d}$.

B. Iterative algorithm (IA)

The performance of NIA degrades at high SNR levels, as indicated in section V. To tackle this issue, we introduce an iterative algorithm (IA), which iterates between CE and symbol detection. The algorithm initiates with the symbol estimate $\hat{\boldsymbol{x}}_d^{(0)} = \hat{\boldsymbol{x}}_{\text{d-NIA}}$ obtained from NIA. Using $\hat{\boldsymbol{x}}_d^{(0)}$, we can compute an initial estimate $\boldsymbol{A}_d^{(0)}$ of $\boldsymbol{A}_d$. The expression for the received signal (6) can be reformulated as

$$\boldsymbol{y}_p = \hat{\boldsymbol{A}}^{(0)}_{\hat{\boldsymbol{x}}_d, \boldsymbol{x}_p} \boldsymbol{h} + \boldsymbol{\gamma}^{(0)}_{\tilde{\boldsymbol{n}}}, \tag{13}$$

where $\hat{\boldsymbol{A}}^{(0)}_{\hat{\boldsymbol{x}}_d, \boldsymbol{x}_p} = \boldsymbol{A}_p + \hat{\boldsymbol{A}}_d^{(0)}$ denotes the data-aided matrix and $\boldsymbol{\gamma}^{(0)}_{\tilde{\boldsymbol{n}}} = (\boldsymbol{A}_d - \hat{\boldsymbol{A}}_d^{(0)})\boldsymbol{h} + \tilde{\boldsymbol{n}} \sim \mathcal{CN}(\boldsymbol{0}, (2(\sum_{i=1}^{P} \sigma^2_{h_i^2})\sigma_d^2 + \sigma^2)\boldsymbol{I}_K)$ is the noise-plus-interference vector.

The estimate of $\boldsymbol{h}$ in the n-th iteration of IA is given by

$$\hat{\boldsymbol{h}}_{\text{IA}}^{(n)} = \boldsymbol{\Phi}^{(n)} \left(\hat{\boldsymbol{A}}^{(n-1)}_{\hat{\boldsymbol{x}}_d, \boldsymbol{x}_p}\right)^H \left(\boldsymbol{C}^{(n-1)}_{\boldsymbol{\gamma}_{\tilde{\boldsymbol{n}}}}\right)^{-1} \boldsymbol{y}_p, \tag{14}$$

where $\boldsymbol{\Phi}^{(n)} = \left(\left(\hat{\boldsymbol{A}}^{(n-1)}_{\hat{\boldsymbol{x}}_d, \boldsymbol{x}_p}\right)^H \left(\boldsymbol{C}^{(n-1)}_{\boldsymbol{\gamma}_{\tilde{\boldsymbol{n}}}}\right)^{-1} \hat{\boldsymbol{A}}^{(n-1)}_{\hat{\boldsymbol{x}}_d, \boldsymbol{x}_p} + \boldsymbol{C}_{\boldsymbol{h}}^{-1}\right)^{-1}$.

Once $\boldsymbol{h}$ is estimated, the effective channel matrix in the n-th iteration can be computed as $\hat{\boldsymbol{H}}^{(n)}_{\text{eff-IA}} = (\boldsymbol{F}_N \otimes \boldsymbol{I}_M)\left(\sum_{i=1}^{P} \hat{h}_i^{(n)} \boldsymbol{\Pi}^{l_i} \boldsymbol{\Delta}^{(k_i)}\right)(\boldsymbol{F}_N^H \otimes \boldsymbol{I}_M)$.

We now employ the proposed simplicity-based detector in (12) to detect the symbol vector. The received signal for symbol detection in the n-th iteration of IA is obtained as

$$\boldsymbol{y}_d^{(n)} = \boldsymbol{y} - \hat{\boldsymbol{H}}^{(n)}_{\text{eff-IA}} \boldsymbol{x}_p = \boldsymbol{H}_{\text{eff}} \boldsymbol{x}_d + \tilde{\boldsymbol{v}}_e^{(n)}, \tag{15}$$

where $\tilde{\boldsymbol{v}}_e^{(n)} = (\boldsymbol{H}_{\text{eff}} - \hat{\boldsymbol{H}}^{(n)}_{\text{eff-IA}})\boldsymbol{x}_p + \tilde{\boldsymbol{n}}$.

From (15), the symbol vector at the n-th iteration of IA $\boldsymbol{x}_d^{(n)}$ can be found by resolving the following problem

$$\begin{aligned} \hat{\boldsymbol{g}}^{(n)} &= \arg\min_{\boldsymbol{g}} ||\underline{\boldsymbol{y}_d}^{(n)} - \underline{\boldsymbol{H}_{\text{eff-IA}}}^{(n)} \boldsymbol{B}_\alpha \boldsymbol{g}^{(n)}||_2 \\ &\text{st. } \boldsymbol{B}_1 \boldsymbol{g}^{(n)} = \boldsymbol{1}_{2MN}, \boldsymbol{g}^{(n)} \geq 0, \end{aligned} \tag{16}$$

where $\boldsymbol{g}^{(n)} \in \mathbb{R}^{4MN}$ is the sparse transform of $\underline{\boldsymbol{x}_d}^{(n)}$: $\underline{\boldsymbol{x}_d}^{(n)} = \boldsymbol{B}_\alpha \boldsymbol{g}^{(n)}$. $\boldsymbol{B}_\alpha = \boldsymbol{I}_{2MN} \otimes [\alpha_1, \alpha_m]$, $\boldsymbol{B}_1 = \boldsymbol{I}_{2MN} \otimes [1, 1]$.

IA iterates between LMMSE-based CE in (14) and simplicity-based data detection in (16) until $|\hat{\boldsymbol{h}}^{(n)} - \hat{\boldsymbol{h}}^{(n-1)}| < \epsilon$ or when the maximum number of iterations N_{max} is reached.

The proposed IA is summarized in Algorithm 1.

IV. Complexity analysis

EP and SP schemes use the MP algorithm for data detection, its cost is $\mu_d = n_{iter} NM|\mathcal{A}|P$ over n_{iter} iterations.

The computational complexity of the simplicity-based detector stems from solving problem (16) using the interior point method. This method's complexity is influenced by the number of constraints and the vector dimension. A convex optimization problem in $\mathbb{R}^m$ with d constraints typically requires $\mathcal{O}(\sqrt{d})$ iterations and $\mathcal{O}(m^2 d)$ computations per iteration, totaling

Algorithm 1 Iterative algorithm for CE and symbol detection.

Input: $\boldsymbol{y} \in \mathbb{C}^{MN\times 1}$, $\boldsymbol{x}_p \in \mathbb{C}^{MN\times 1}$, σ^2

Initializations: initial symbol detection: $\hat{\boldsymbol{x}}_d^{(0)} = \hat{\boldsymbol{x}}_{\text{d-NIA}}$ obtained from NIA, counter: $n = 1$.

repeat

Compute $\hat{\boldsymbol{h}}_{\text{IA}}^{(n)} = \boldsymbol{\Phi}^{(n)} \left(\hat{\boldsymbol{A}}_{\hat{\boldsymbol{x}}_d,\boldsymbol{x}_p}^{(n-1)}\right)^H \left(\boldsymbol{C}_{\boldsymbol{\gamma}_{\tilde{\boldsymbol{n}}}}^{(n-1)}\right)^{-1} \boldsymbol{y}_p$,

Compute $\boldsymbol{y}_d^{(n)} = \boldsymbol{y} - \hat{\boldsymbol{H}}_{\text{eff-IA}}^{(n)} \boldsymbol{x}_p = \boldsymbol{H}_{\text{eff}} \boldsymbol{x}_d + \tilde{\boldsymbol{v}}_e^{(n)}$,

Compute $\hat{\boldsymbol{x}}_d$ by feeding the simplicity-based detector with $\hat{\boldsymbol{H}}_{\text{eff-IA}}^{(n)}$ and $\boldsymbol{y}_d^{(n)}$,

Compute $\hat{\boldsymbol{h}}_{\text{IA}}^{(n+1)}$ with the following noise approximation: $\boldsymbol{\gamma}_{\tilde{\boldsymbol{n}}}^{(n)} \sim \mathcal{CN}\left(\boldsymbol{0}, \left(2\left(\sum_{i=1}^{P} \sigma_{h_i^2}^2\right)\sigma_d^2 + \sigma^2\right)\boldsymbol{I}_K\right)$

until $|\hat{\boldsymbol{h}}^{(n)} - \hat{\boldsymbol{h}}^{(n-1)}| > \epsilon$ or $n = N_{max}$.

Output: $\hat{\boldsymbol{h}}$, $\hat{\boldsymbol{x}}_d$.

$\mathcal{O}(m^2 d)$ [11]. Applied to our problem, the simplicity-based detector's overall cost is $(NM)^3$.

The computational complexity of CESD is $C_{\text{CESD}} = N_{iter}(\mathcal{O}(\mu_1) + \mathcal{O}(\mu_2))$, where μ_1 and μ_2 are the costs of the CE and symbol detection steps. For the CE step using an LMMSE estimator, which require the inversion of a $P \times P$ matrix, the cost is dominated by $\mu_1 = P^3$. Thus, the CESD's complexity is $C_{CESD} = N_{iter}\mathcal{O}(P^3) + \mathcal{O}(N^3M^3)$.

The complexity of the EP algorithm is dominated by $C_{\text{EP}} = \mathcal{O}(Nl_\tau) + \mathcal{O}(\mu_d)$, while that of the SP algorithm is $C_{\text{SP}} = 2\mathcal{O}(\mu_e)$, where $\mu_e = (4P^2 + 6L)MN + (P^3 + L)$ [8].

In practical scenarios where $P, L, l_\tau \ll MN$, the complexities of CESD, EP, and SP algorithms are dominated by $C_{\text{CESD}} = N_{iter}\mathcal{O}((NM)^3)$, $C_{\text{EP}} = \mathcal{O}(n_{iter}NMAP)$, and $C_{\text{SP}} = (n_s + 1)\mathcal{O}(MN) + n_s\mathcal{O}(n_{iter}NMAP)$.

In conclusion, the EP scheme offers the lower complexity due to its use of GI to mitigate pilot-data interference. However, this comes at the expense of reduced SE. Our proposed CESD, while introducing additional computational complexity, effectively reduces the overall CE complexity while improving BER performance. Additionally, CESD's complexity is independent of $|\mathcal{A}|$, unlike for the SP design.

V. Simulation results

In this section, we evaluate the performance of CESD concerning SE, NMSE, and BER in high-mobility scenarios. We then compare these performance metrics with various existing methods, including several state-of-the-art techniques.

A. Simulation parameters

The delay and Doppler bins are given as $N = M = 16$. The carrier frequency is $f_c = 4$ GHz and the subcarrier spacing is $\Delta f = 15$ KHz. QPSK constellation is used. We employ the 5-path DD channel model. The maximum delay shift is $\tau_{max} = 20.8\ \mu s$, corresponding to a maximum delay tap $l_\tau = 5$ and the maximum Doppler shift is $\nu_{max} = 1850$ Hz, indicating a high-mobility scenario with a maximum Doppler tap $k_\nu = 2$ and a maximum speed of $v_{max} = 500$ km/h.

TABLE I: Pilot overhead comparison between CESD and state-of-the-art methods ($M = N = 16$, $K_p = 4$, $L_p = 30$, and $N_G = 98$, $v_{max} = 500$ km/h).

Design	Pilot overhead (η_s)	η_s value
CPA [3]	$(MN/2MN)$	0.5
EP [1]	$((N_G+1)/MN)$	0.39
RG-BL [5]	$(K_p/(K_p+N))$	0.2
BSBL-BR [6] NGR [7]	(L_p/MN)	0.12
SP [8]	$(L_p + (N_f-1)(0))/(MNN_f)$	0.012
Proposed (CESD)	$(L_p + (N_f-1)(0))/(MNN_f)$	0.012

The channel used conforms to a DU channel [8]. The number of frames N_f in which the delay and Doppler taps remain constant is given by $N_f = T_s/T_f$, where $T_f = N/\Delta f$ is the frame duration. In this case, $N_f \approx 10$. The value of N_f increases as v_{max} decreases: for $v_{max} = 250$ km/h, $N_f \approx 20$.

Our approach involves first estimating $\{l_i, k_i\}_{i=1:P}$ using the simple threshold method and the NGR scheme [13] in the initial frame. In the subsequent $N_f - 1$ frames, CESD is employed to estimate $\{h_i\}_{i=1:P}$. Consequently, the expression for the SE is $\mathcal{R}_{\text{CESD}} = (\mathcal{R}_{\text{NGR}} + (N_f - 1)\mathcal{R}_{\text{SP}})/N_f$, where $\mathcal{R}_{\text{NGR}}$ and $\mathcal{R}_{\text{SP}}$ denote the SE of the NGR and SP schemes.

B. SE performance

The SE of a scheme s is given by $\mathcal{R} = (1 - \eta_s)\log_2(|\mathcal{A}|)$, where η_s is the pilot overhead of s. Consequently, for a given alphabet $\mathcal{A}$, as the pilot overhead increases, the SE decreases, and vice versa.

Table I presents the pilot overhead of CESD and state-of-the-art schemes. Unlike other schemes, CESD does not use GI and distributes data symbols across all locations in the DD grid, minimizing pilot overhead. Analyzing Table I, we observe that CESD performs similarly as SP design and outperforms all the other state-of-the-art methods. This superiority is attributed to the superposition of K pilots onto data symbols in a sub-grid of the DD grid without using GI.

C. NMSE performance

Figure 2a depicts the NMSE performance of CESD (NIA), CESD (IA), SP-I [8] method, and the two-stages [7] design. From the figure, it is shown that the performance of CESD (NIA) is degraded compared to other methods. This degradation can be attributed to imprecise CE resulting from pilot-symbol interferences. On the other hand, CESD (IA) outperforms all the methods and surpasses the two-stages algorithm by approximately 1 for SNR $= 10$ dB. This performance gain is achieved by minimizing interferences through the proposed strategic allocation of pilots and data symbols.

D. BER performance

Figure 2b illustrates the BER versus SNR of CESD as a function of K/NM. This figure was obtained using the following values of M_p and N_p: $5 \leq M_p \leq 16$ and $2 \leq N_p \leq 7.5$. It is shown that the CE accuracy increases with the rise in the number of pilots. However, in this superimposed scheme, as

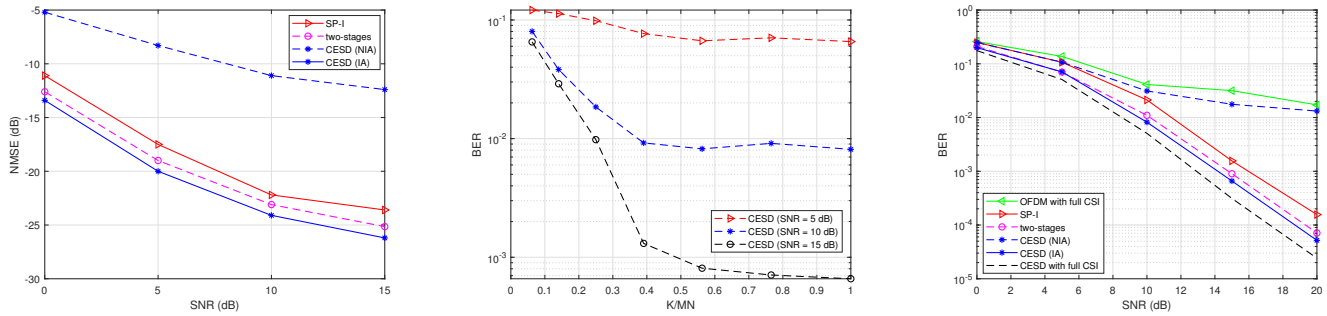

(a) (b) (c)

Fig. 2: (a) NMSE versus SNR performance. (b) BER versus $\frac{K}{MN}$. (c) BER versus SNR performance.

the number of pilots increases, interference with data symbols also increases, leading to a degradation in symbol detection probability. Additionally, the computational complexity of CE increases with the growing of pilots number.

Based on these observations, we opted to determine the minimal number of pilots that allows for effective data symbol detection while reducing the computational complexity of CE. From Fig. 2b, it is noticeable that beyond $K/MN = 0.5$, the BER remains relatively constant. Therefore, by selecting $K = 0.5NM$ pilots, we achieve similar BER performance compared to a higher number of pilots. This approach helps in reducing the computational complexity during the CE step.

We now analyze the BER-SNR performance in Fig 2c, comparing CESD to SP design [8], two-stages method [7], OFDM with perfect CSI and CESD with perfect CSI. It is shown that the BER of the OTFS system, with the proposed designs, is significantly lower than that of the OFDM system. It is also shown from the figure that CESD and two-stages method exhibit similar performance. Remarkably, CESD outperforms all other methods, demonstrating performance close to CESD with perfect CSI. It surpasses SP-I by 3 dB at a BER of 10^{-4}. This gain is ensured by not superimposing all the data symbols with the pilots, minimizing interferences. In addition to the gain in terms of PAPR compared with schemes using GI, the proposed PSP pilot pattern and CESD algorithm achieves a good balance between computational complexity, SE and BER performance compared to state-of-the-art schemes.

VI. Conclusion

In this paper, we have proposed a pilot pattern called partially superimposed pilots scheme for OTFS system. This novel approach strategically balance computational complexity and channel estimation (CE) accuracy. We also proposed an iterative algorithm for CE and symbol detection, called CESD. This algorithm employ linear minimum mean squared error for CE and simplicity-based detection in an iterative way. Simulation results, conducted under high-mobility environments, have shown that the proposed scheme achieves a good compromise between bit error rate, spectral efficiency, PAPR, and computational complexity.

References

[1] P. Raviteja, K. T. Phan, and Y. Hong, "Embedded pilot-aided channel estimation for OTFS in delay–doppler channels," *IEEE transactions on vehicular technology*, vol. 68, no. 5, pp. 4906–4917, 2019.

[2] A. Monk, R. Hadani, M. Tsatsanis, and S. Rakib, "OTFS-orthogonal time frequency space," *arXiv preprint arXiv:1608.02993*, 2016.

[3] M. K. Ramachandran and A. Chockalingam, "MIMO-OTFS in high-doppler fading channels: Signal detection and channel estimation," in *IEEE Global Communications Conference (GLOBECOM)*, pp. 206–212, 2018.

[4] R. Ouchikh, A. Aïssa-El-Bey, T. Chonavel, and M. Djeddou, "Sparse channel estimation algorithms for OTFS system," *IET Communications*, vol. 16, no. 18, pp. 2158–2170, 2022.

[5] S. Srivastava, R. K. Singh, A. K. Jagannatham, and L. Hanzo, "Bayesian learning aided simultaneous row and group sparse channel estimation in orthogonal time frequency space modulated MIMO systems," *IEEE Transactions on Communications*, vol. 70, no. 1, pp. 635–648, 2021.

[6] L. Zhao, J. Yang, Y. Liu, and W. Guo, "Block sparse bayesian learning-based channel estimation for MIMO-OTFS systems," *IEEE Communications Letters*, vol. 26, no. 4, pp. 892–896, 2022.

[7] R. Ouchikh, A. Aïssa-El-Bey, T. Chonavel, and M. Djeddou, "Joint channel estimation and symbol detection for OTFS system using a two-stage algorithm," in *57th Asilomar Conference on Signals, Systems, and Computers*, 2023.

[8] H. B. Mishra, P. Singh, A. K. Prasad, and R. Budhiraja, "OTFS channel estimation and data detection designs with superimposed pilots," *IEEE Transactions on wireless communications*, vol. 21, no. 4, pp. 2258–2274, 2021.

[9] R. Ouchikh, A. Aïssa-El-Bey, T. Chonavel, and M. Djeddou, "Iterative channel estimation and data detection algorithm for OTFS modulation," in *IEEE International Conference on Acoustics, Speech and Signal Processing (ICASSP)*, pp. 5263–5267, 2022.

[10] R. Ouchikh, A. Aissa-El-Bey, T. Chonavel, and M. Djeddou, "Alternative threshold-based channel estimation and message-passing-based symbol detection in MIMO-OTFS systems using superimposed pilots," *Physical Communication*, vol. 59, p. 102091, 2023.

[11] Z. Hajji, A. Aïssa-El-Bey, and K. Amis, "Simplicity-based recovery of finite-alphabet signals for large-scale MIMO systems," *Digital Signal Processing*, vol. 80, pp. 70–82, 2018.

[12] N. Lassami, A. Aïssa-El-Bey, and K. Abed-Meraim, "Blind joint MIMO channel and data estimation based on regularized ML," *Digital Signal Processing*, vol. 117, p. 103201, 2021.

[13] R. Liu, Y. Huang, D. He, Y. Xu, and W. Zhang, "Optimizing channel estimation overhead for OTFS with prior channel statistics," in *IEEE Wireless Communications and Networking Conference (WCNC)*, pp. 1–6, 2021.